Supplement of Clim. Past, 17, 2653–2677, 2021
https://doi.org/10.5194/cp-17-2653-2021-supplement

Supplement of

Hydroclimatic variability of opposing Late Pleistocene climates in the Levant revealed by deep Dead Sea sediments

Yoav Ben Dor et al.

Correspondence to: Yoav Ben Dor (yoav.bendor1@mail.huji.ac.il)

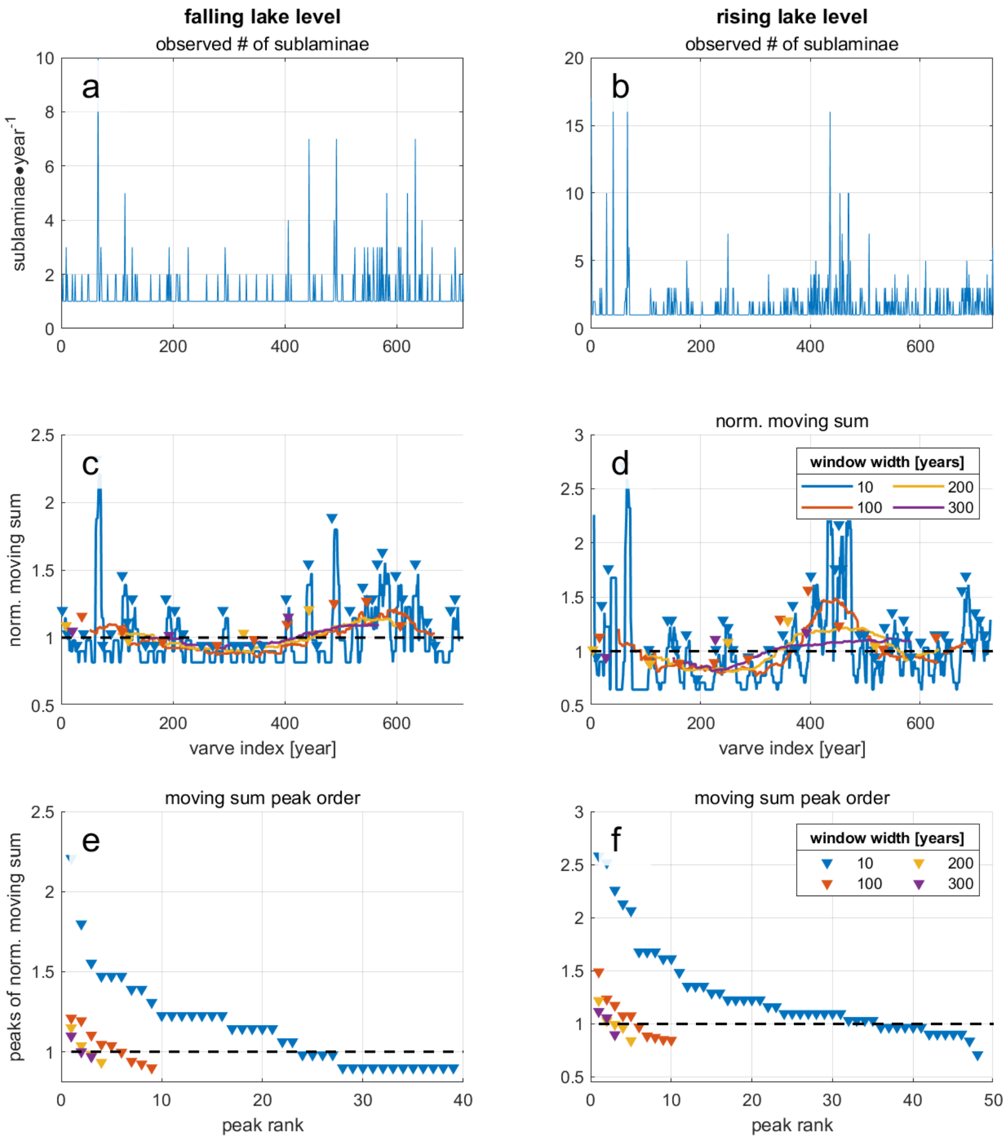

Figure S1 – (a, b) the studied time series of sublaminae. (c, d) the running normalized sum of sublaminae (the $y_{w(i)}$ statistic in main text) calculated using several window widths. Values larger than one are above the mean level. Detected peaks are marked by a triangle. (e, f) the $y_{w(i)}$ values of detected peaks of the $y_{w(i)}$ statistic, ordered by their ranks.

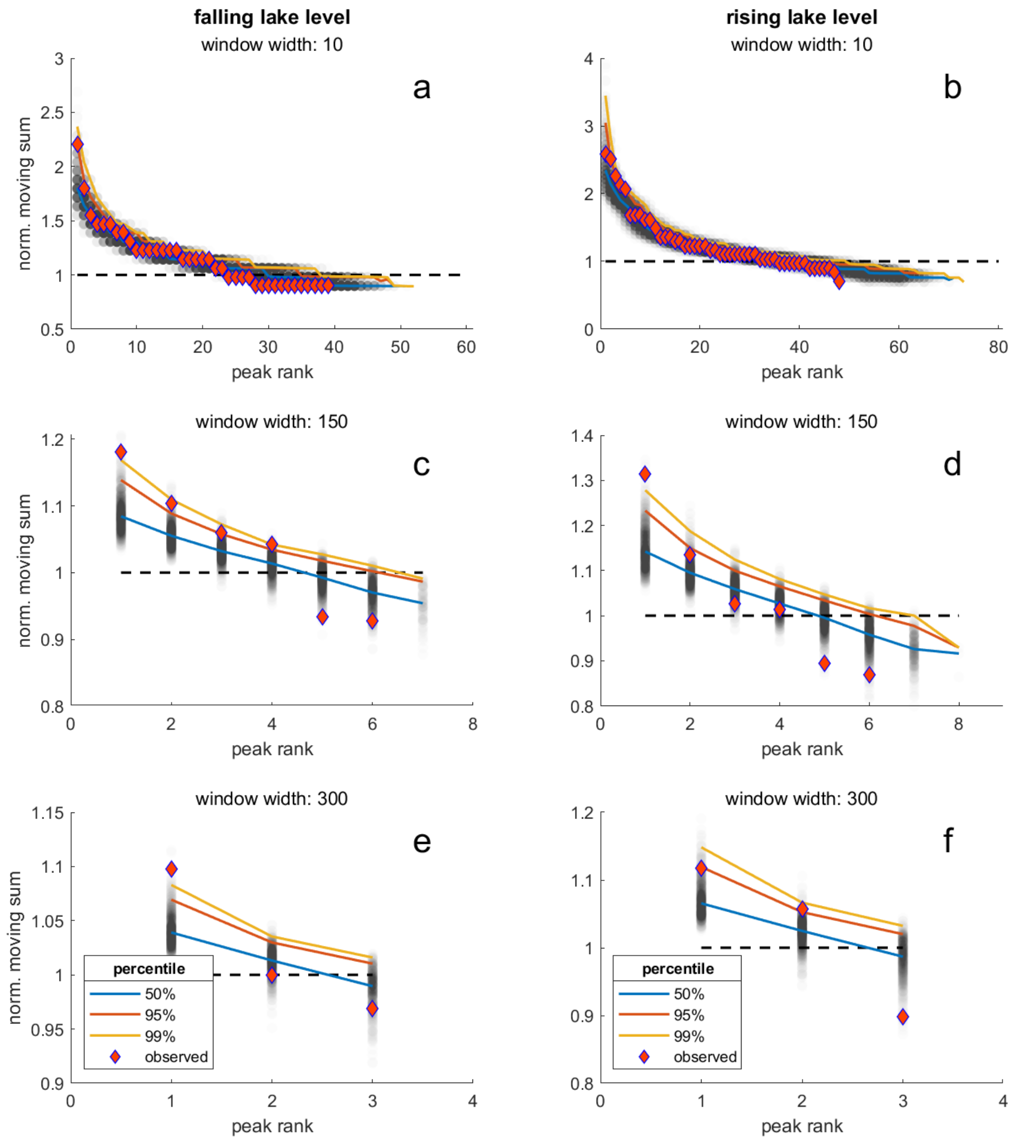

Figure S2 – rank distributions of $y_{w(i)}$ values of peaks calculated using 10,000 randomly permutated series depicting the values of the random series (grey circles), the median, 95th and 99th percentile for each peak order (coloured lines), and the observed value in the studied series using different window widths for falling (left) and rising (right) lake levels. Values significant at α=0.05 plot above the 95th percentile of the randomly permutated series, whereas non-significant values appear below the 95th percentile.

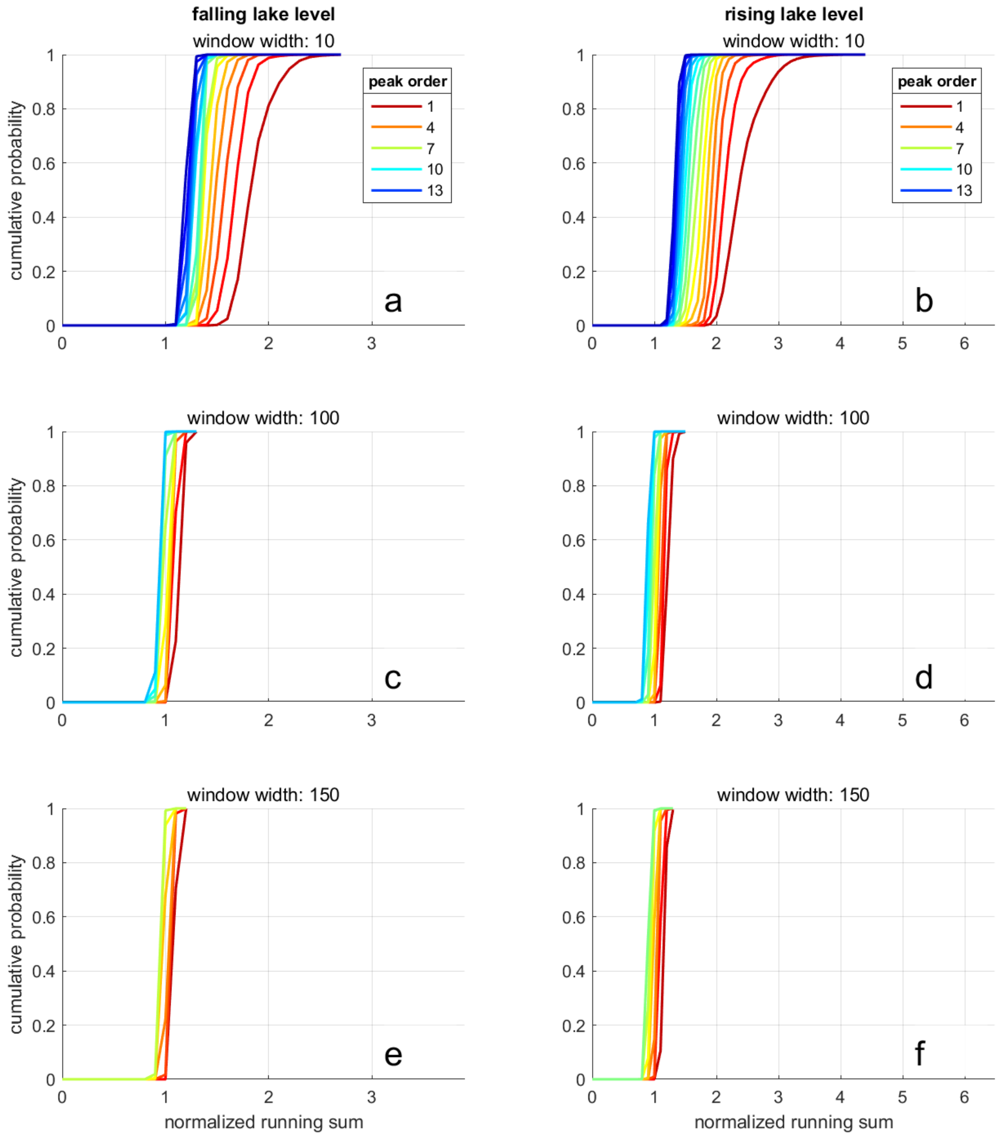

Figure S3 – cumulative distributions of $y_{w(i)}$ values of peaks calculated for 10,000 randomly permutated series depicting the values of the random series for four representative window widths for falling (lefts panels) and rising (right panels) lake levels. Note the decrease in both $y_{w(i)}$ values and the number of identified peaks with increasing window width.

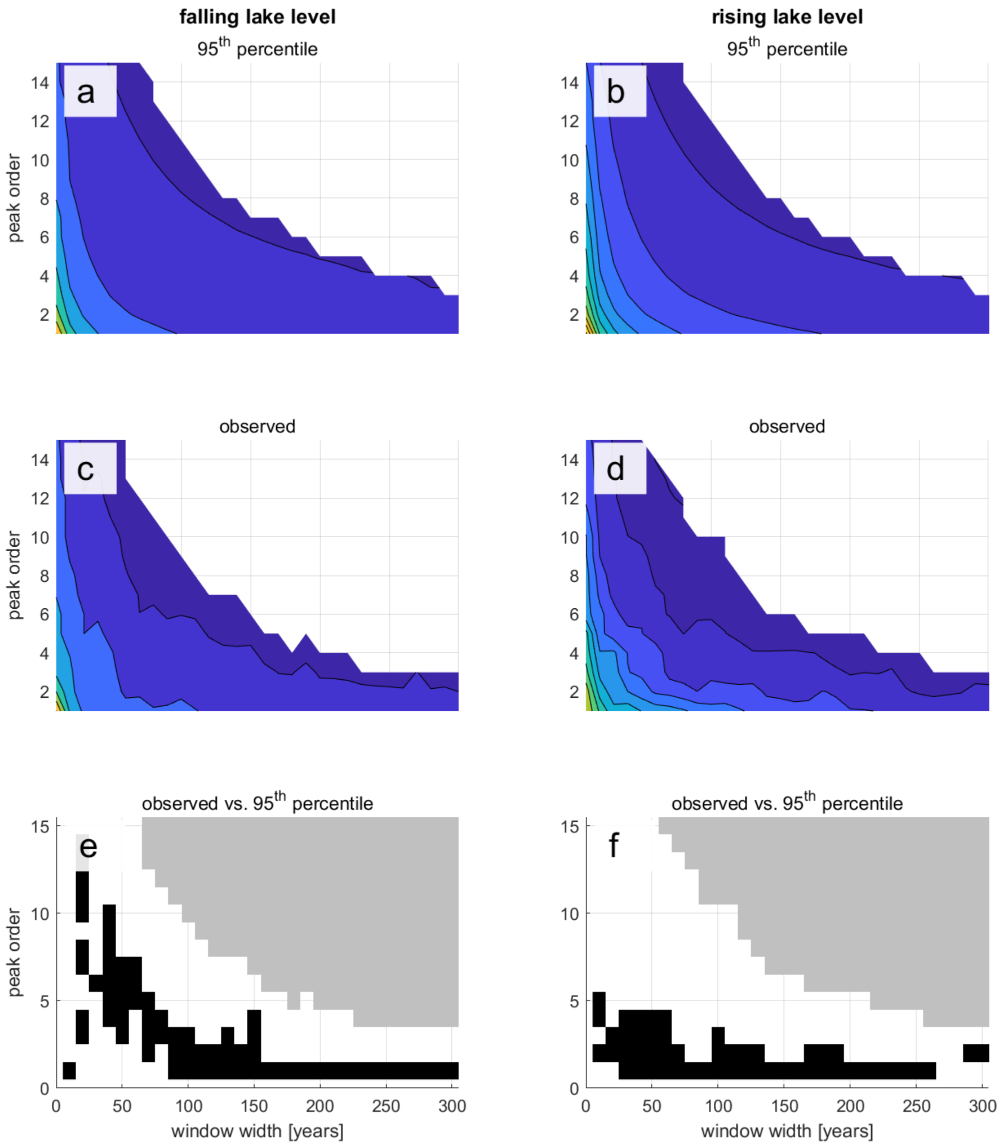

Figure S4 – (a, b) the resulting $\boldsymbol{y}_{(\boldsymbol{w},\boldsymbol{i})}$ values of the 95th percentile for every peak rank (1-15) and window width (10-300). (c, d) the observed $\boldsymbol{y}_{\boldsymbol{w}(\boldsymbol{i})}$ values for every peak rank (1-15) and window width (10-300). (e, f) a binary diagram indicating where observed $\boldsymbol{y}_{\boldsymbol{w}(\boldsymbol{i})}$ values are higher than the calculated 95th percentile of 10,000 randomly permutated series, and are thus statistically significant at α=0.05 (black pixels) or non-significant (white pixels). Missing values, where not enough peaks were detected to calculate the 95th percentile are coded grey. Left and right panels depict results for falling and rising lake levels, respectively.

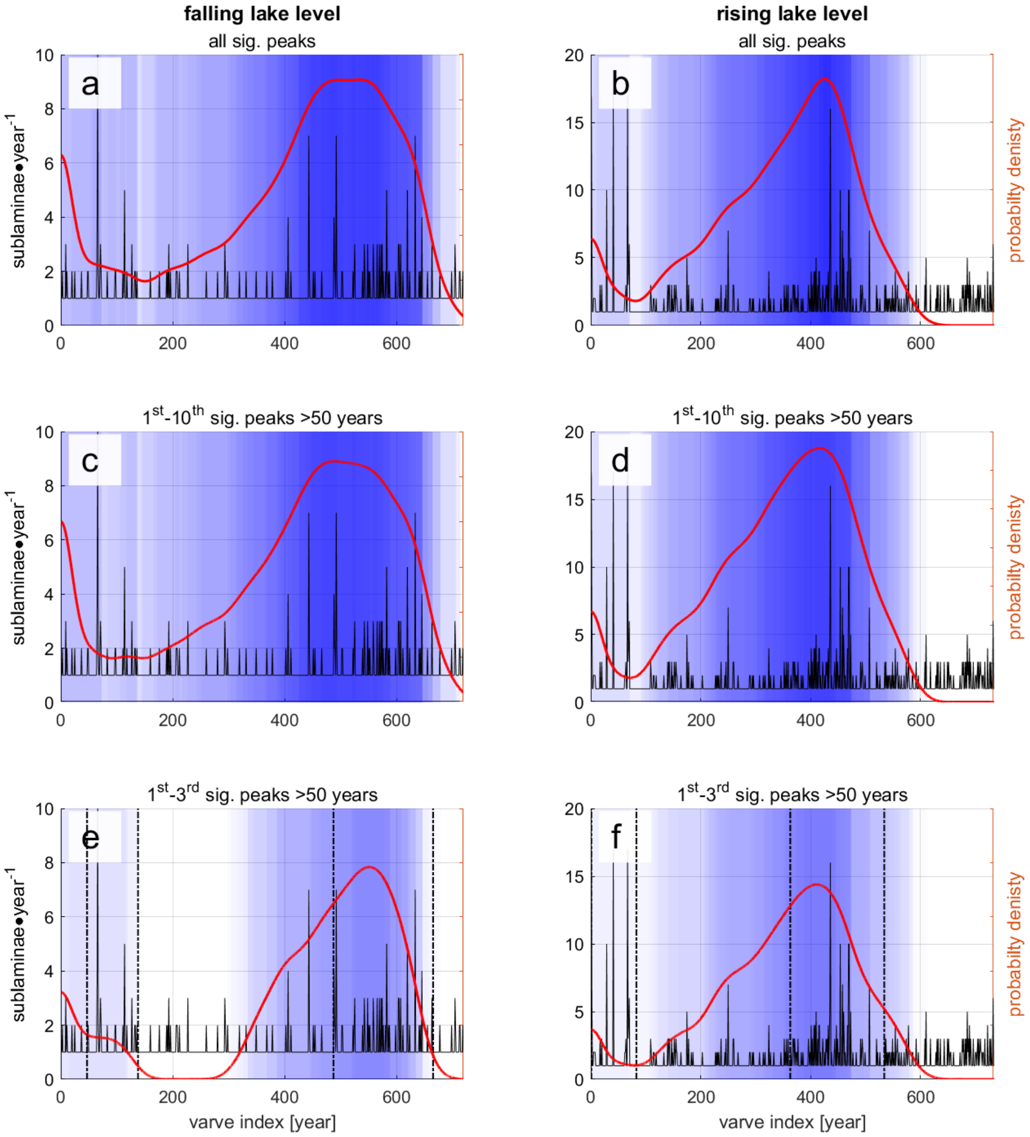

Figure S5 – the location of statistically significant peaks at α=0.05 depicted as semi-transparent shading for: (a, b) all identified statistically significant peaks, (c, d) only peaks detected for window widths longer than 50, and (e, f) for the top five ranking peaks of window widths ranging between 50 and 300 years. Two clusters were identified in each of the studied intervals. The red line depicts the probability of the summed identification of clusters by all window widths selected in each plot, and the identified refined clusters are marked by dashed vertical lines. Left and right panels depict results for falling and rising lake levels, respectively.

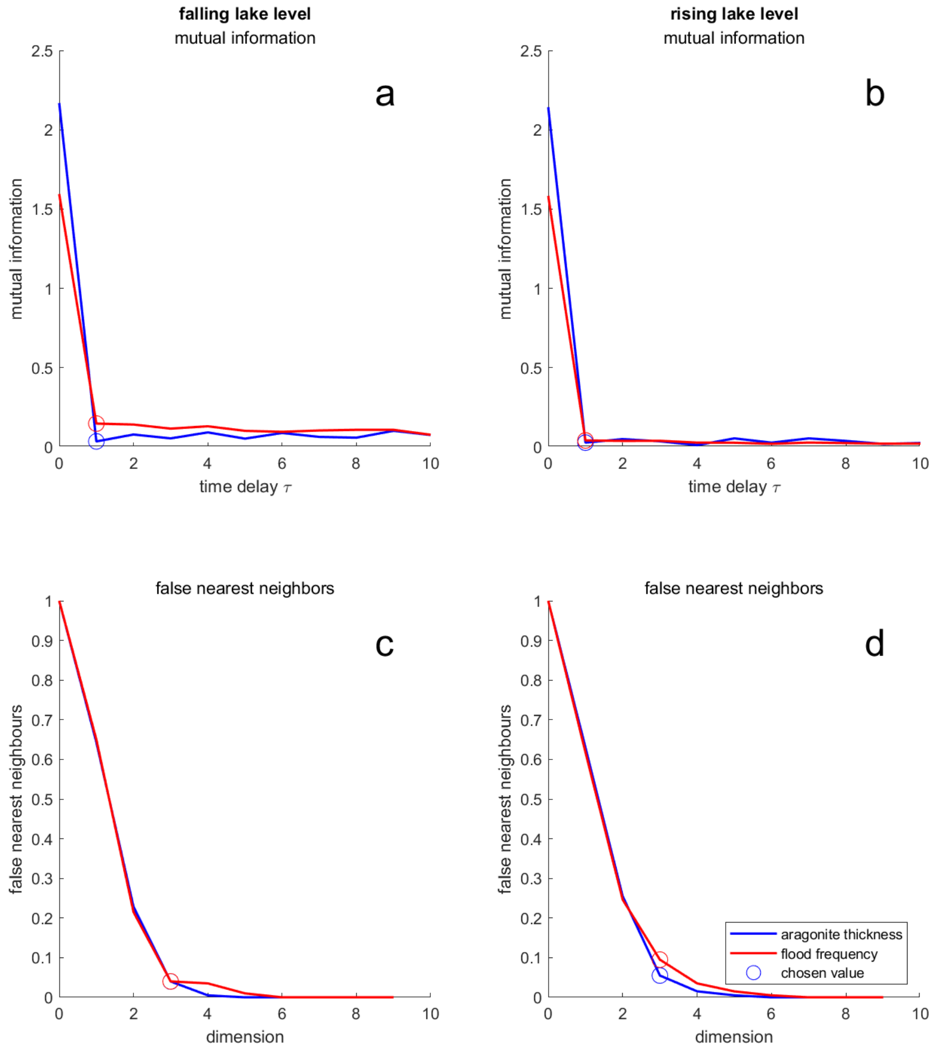

Figure S6 – (c, d) False nearest neighbour analyses of aragonite (blue) and flood frequency (red) during falling (c) and rising (d) lake level. The analyses were performed over the rescaled and normalized data after detrending removing the 1st SSA reconstructed component. (c, d) Results of mutual information analyses of aragonite and flood frequency during falling (c) and rising (d) lake level. The selected parameters for the recurrence analyses are marked with a circle.

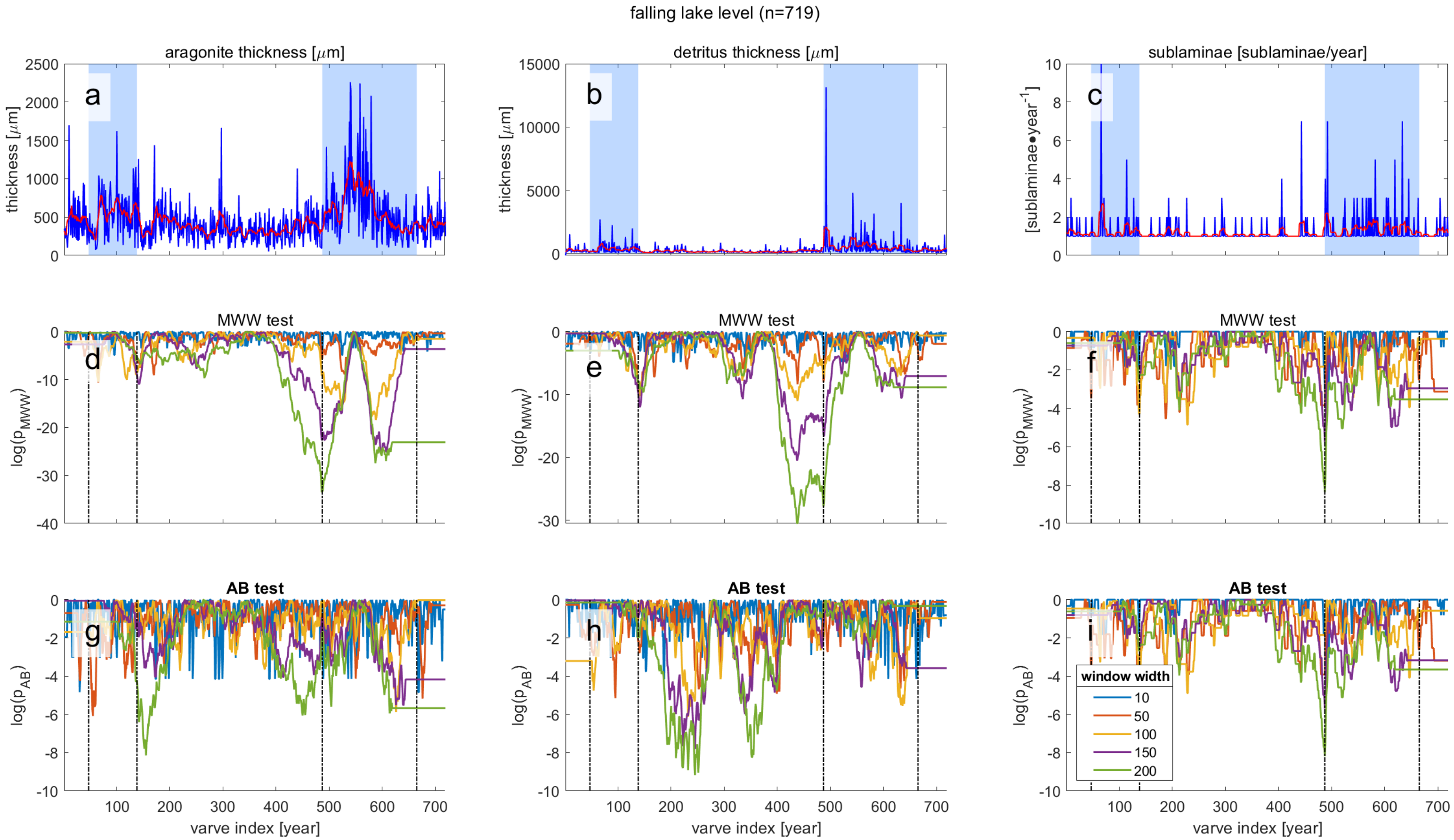

Figure S7 –data and statistical analyses of microfacies results of the core section deposited during lake level fall. (a) thickness of aragonite laminae, (b) thickness of detrital laminae and (c) flood frequency. d-f – log of p-value of running Mann-Whitney-Wilcoxon (MWW) with window widths ranging from 10 to 200. g-i – Ansari-Bradley (AB) test with window widths ranging from 10 to 200. Clusters edges (Fig. 3) were refined based on the results in f and i.

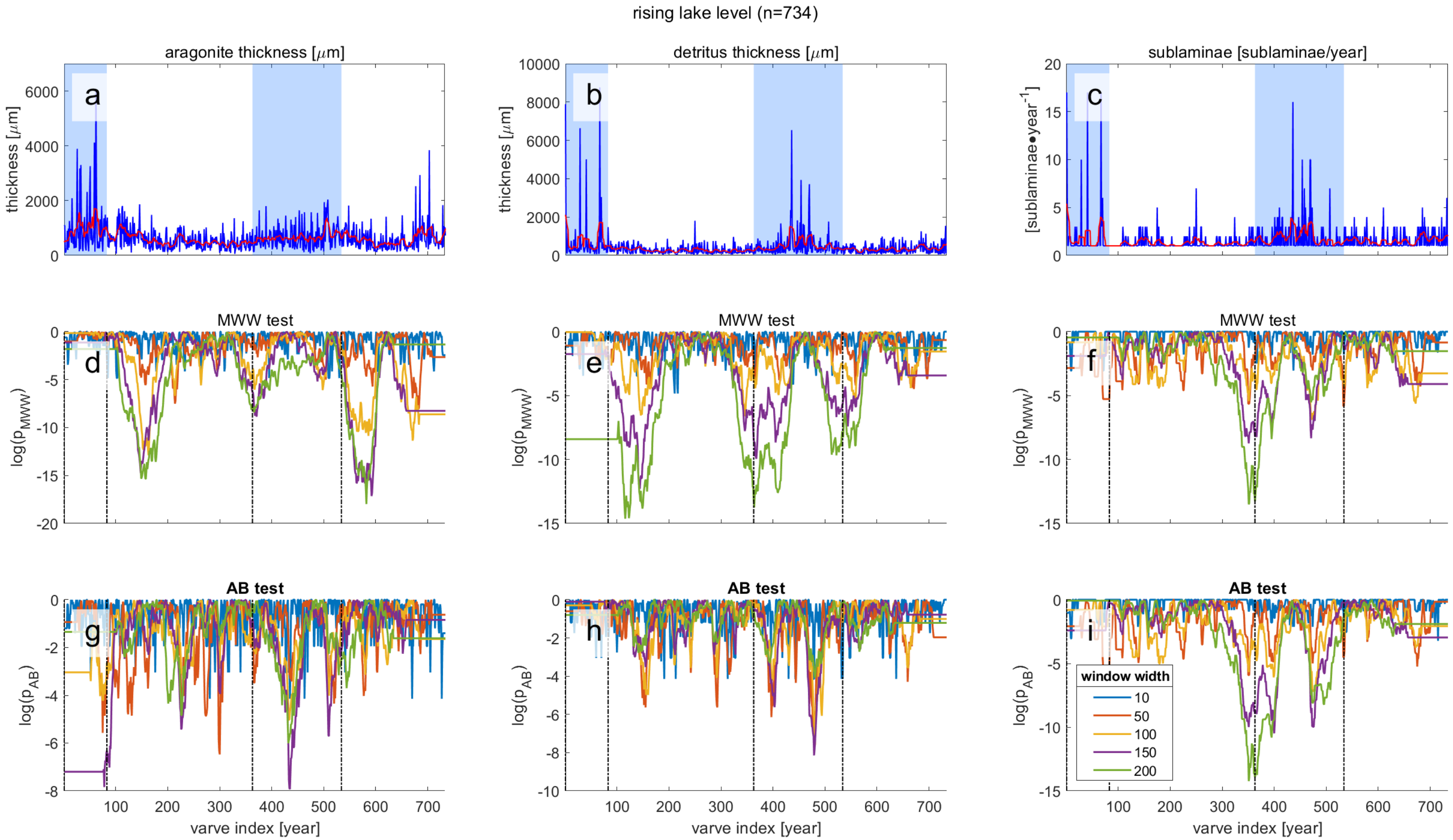

Figure S8 –data and statistical analyses of microfacies results of the core section deposited during lake level rise. (a) thickness of aragonite laminae, (b) thickness of detrital laminae and (c) flood frequency. d-f – log of p-value of running Mann-Whitney-Wilcoxon (MWW) with window widths ranging from 10 to 200. g-i – Ansari-Bradley (AB) test with window widths ranging from 10 to 200. Clusters edges (Fig. 3) were refined based on the results in f and i.

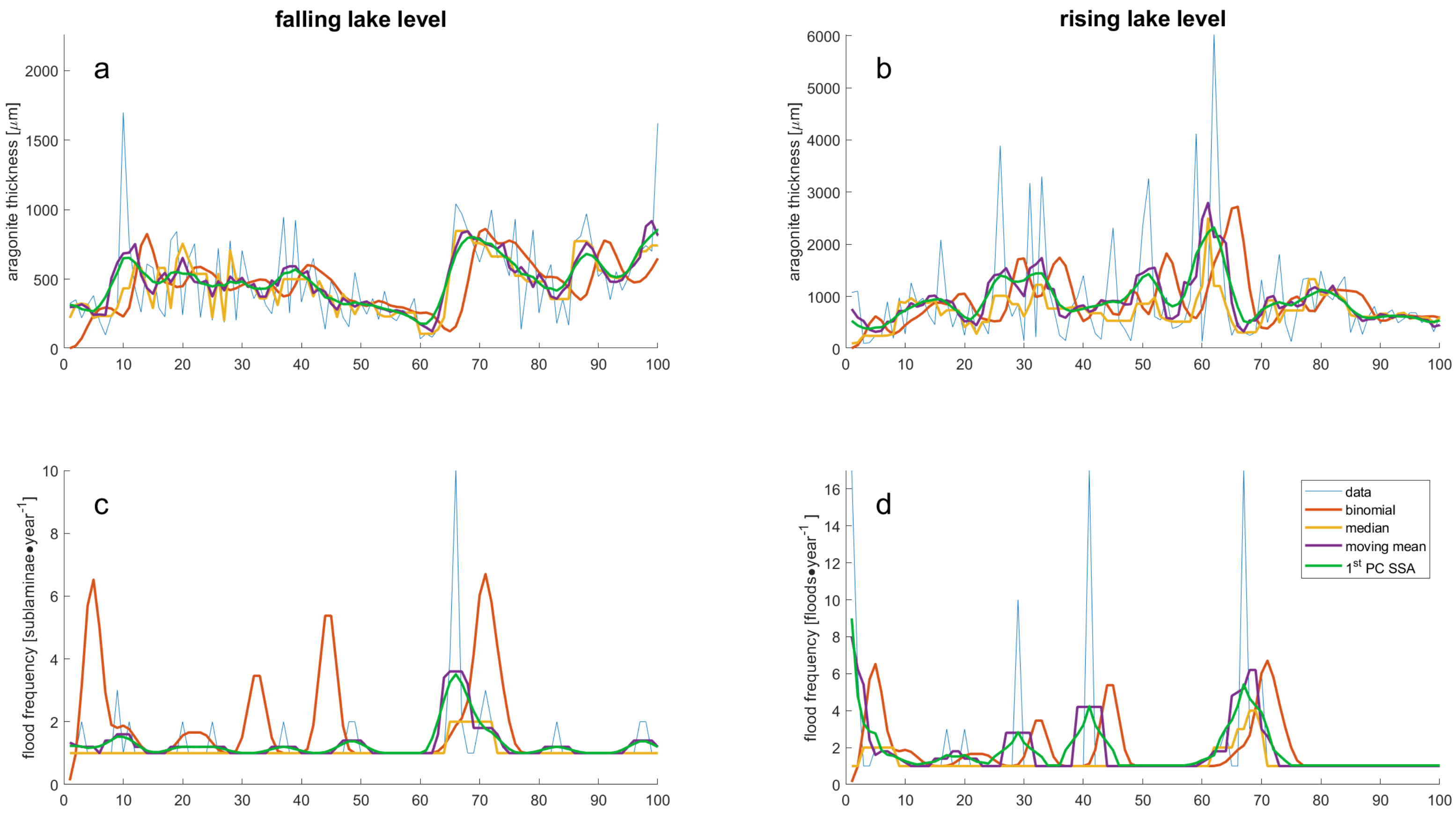
falling lake level
rising lake level
a
b
c
d
aragonite thickness [μm]
flood frequency [sublaminae•year⁻¹]
flood frequency [floods•year⁻¹]
data
binomial
median
moving mean
1st PC SSA

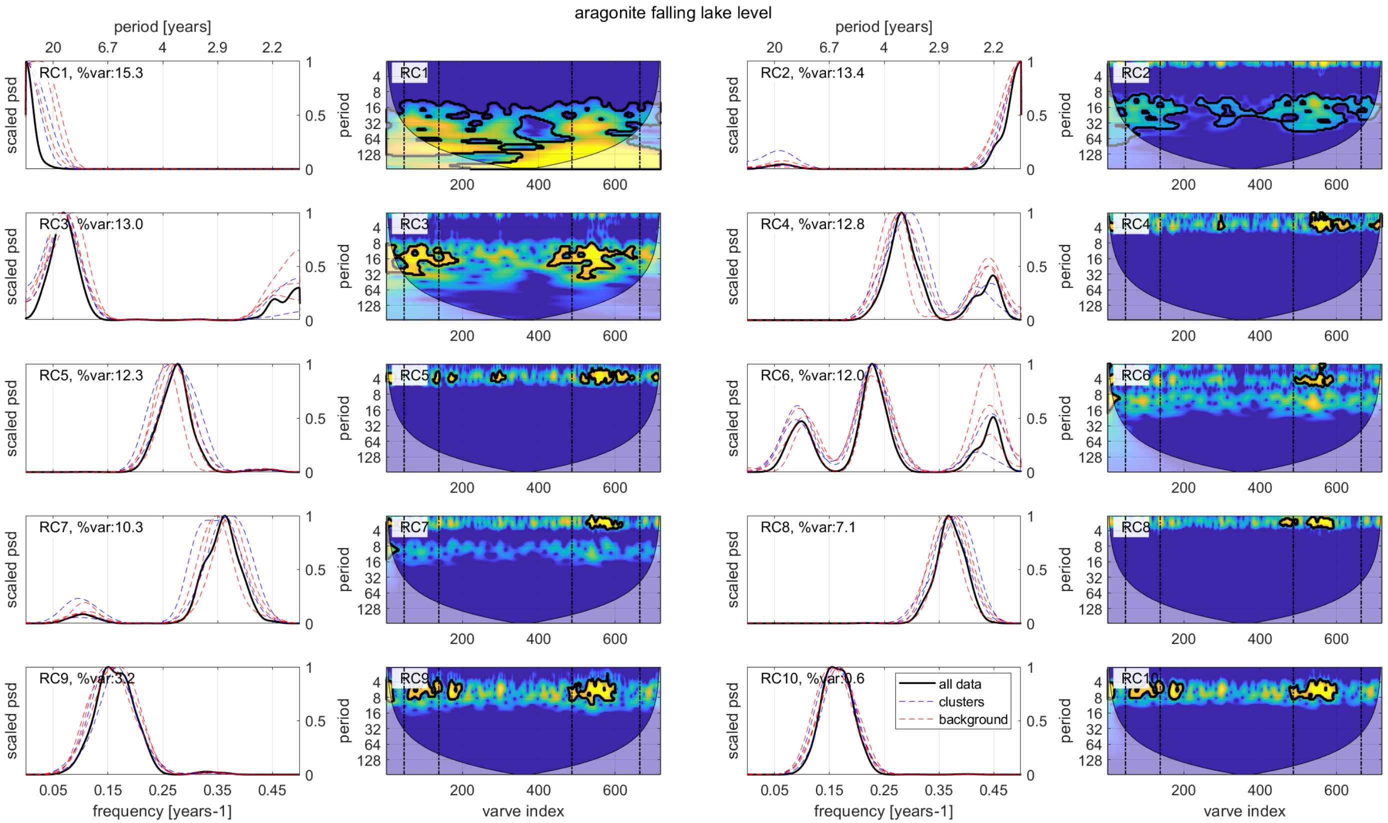

Figure S10 – Welch periodogram and wavelet analyses for the SSA RCs 1-10 of aragonite thickness data during lake level fall. The periodograms were calculated using a Hamming window of 25 years length with 50% overlap, and wavelet analyses were carried out after normalizing to zero mean and a unity standard deviation.

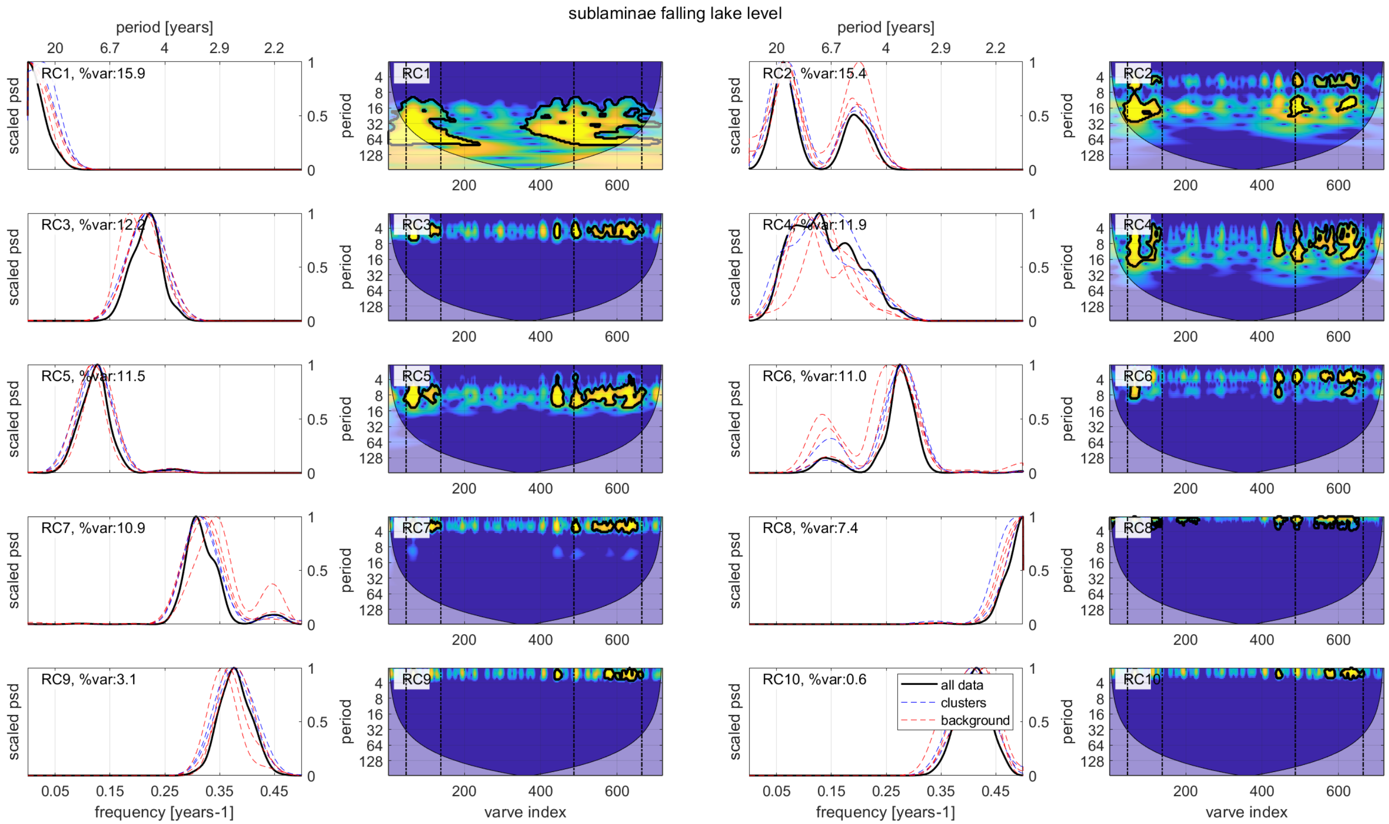

Figure S11 – Welch periodogram and wavelet analyses for the SSA RCs 1-10 of the sublaminae data during lake level fall. The periodograms were calculated using a Hamming window of 25 years length with 50% overlap, and wavelet analyses were carried out after normalizing to zero mean and a unity standard deviation.

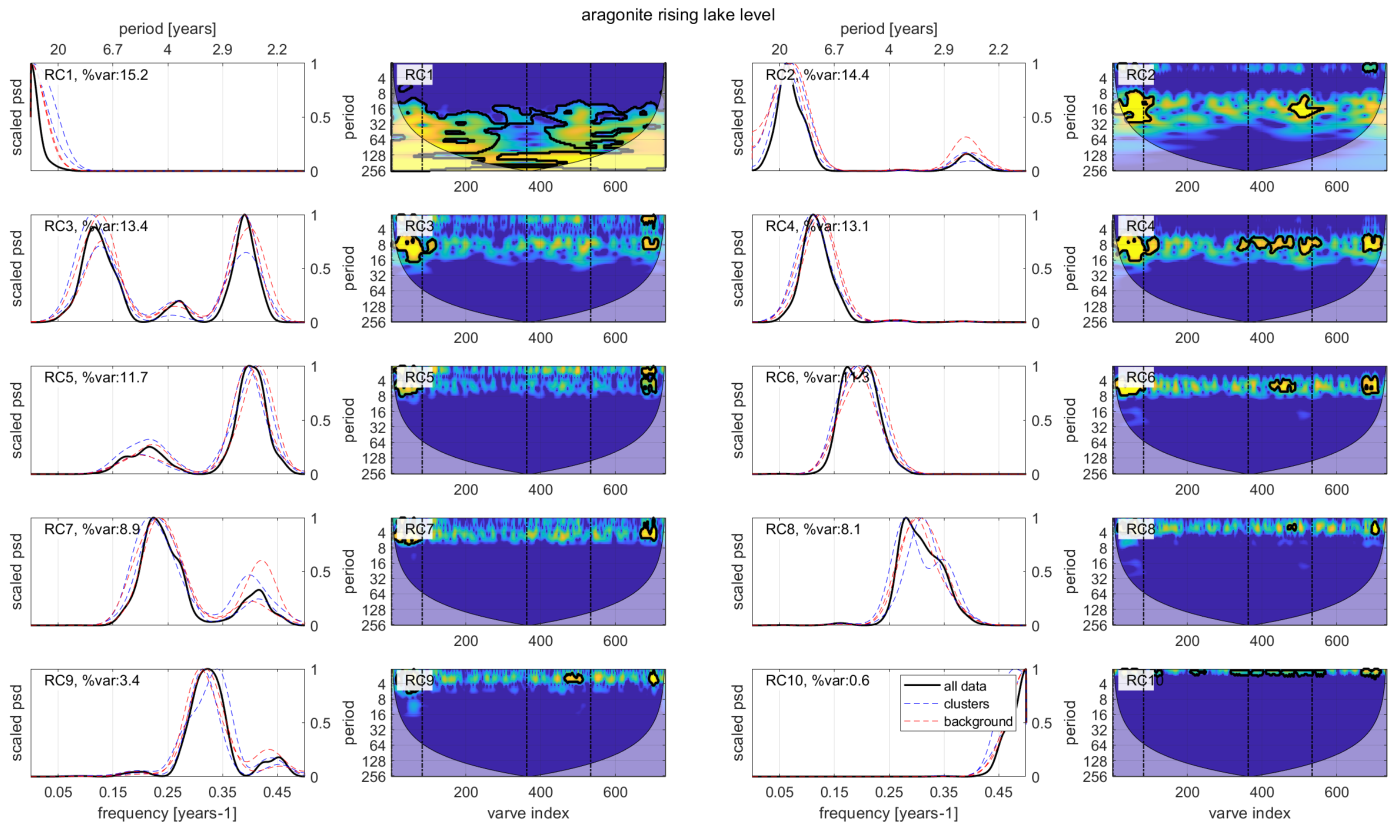

Figure S12 – Welch periodogram and wavelet analyses for the SSA RCs 1-10 of the aragonite thickness data during lake level rise. The periodograms were calculated using a Hamming window of 25 years length with 50% overlap, and wavelet analyses were carried out after normalizing to zero mean and a unity standard deviation.

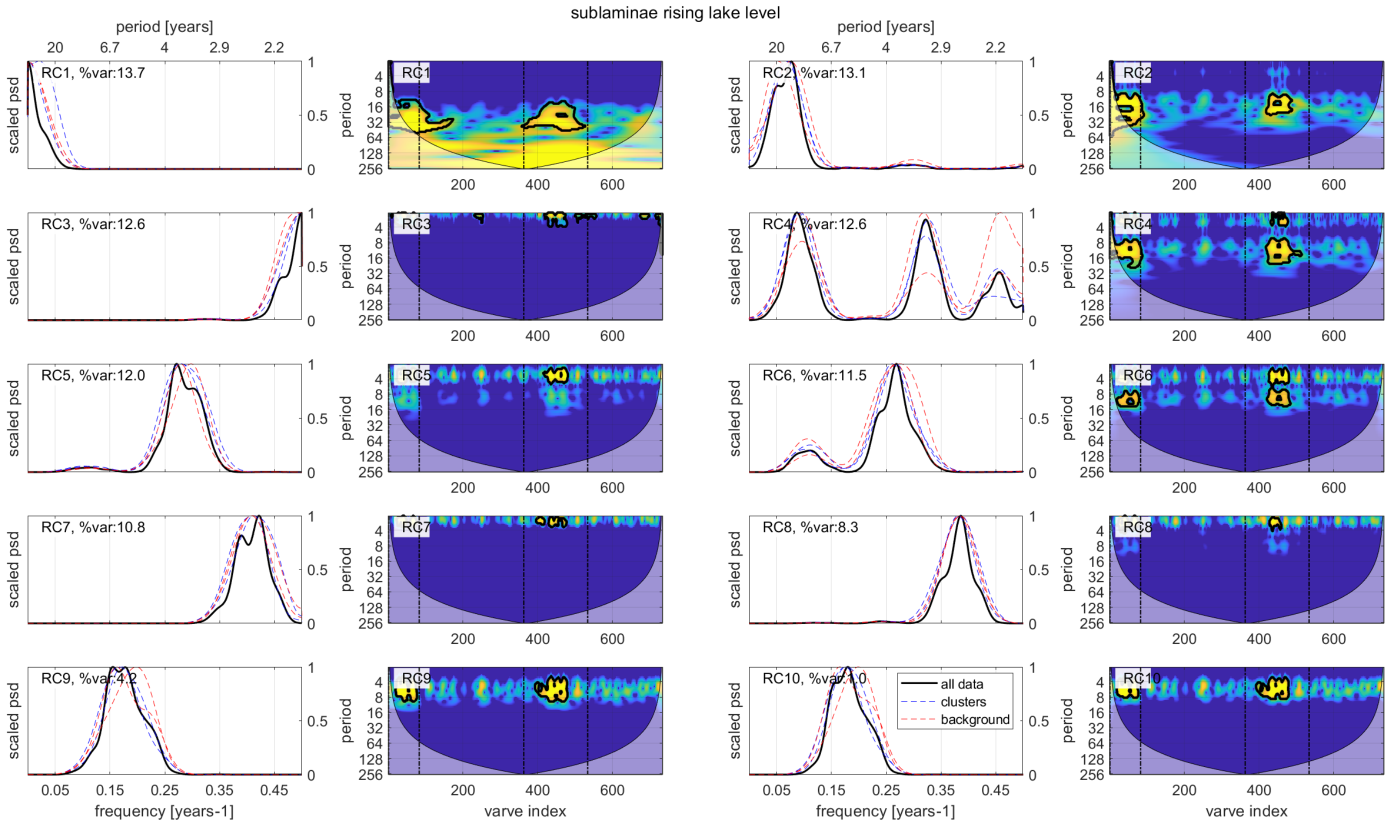

Figure S13 – Welch periodogram and wavelet analyses for the SSA RCs 1-10 of the sublaminae data during lake level rise. The periodograms were calculated using a Hamming window of 25 years length with 50% overlap, and wavelet analyses were carried out after normalizing to zero mean and a unity standard deviation.

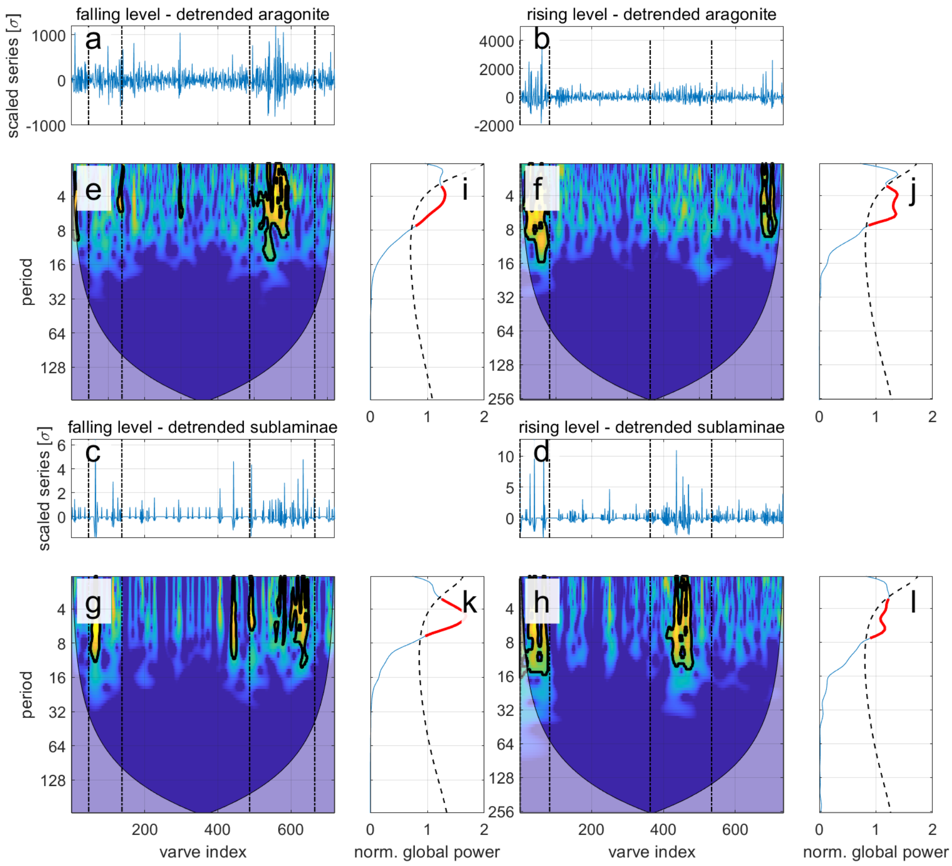

Figure S14 – wavelet and global-wavelet spectra of detrended aragonite thickness and flood frequency during falling (left) and rising (right) episodes. Periodicities with significance level above 0.95 (alpha=0.05) are depicted by a black line. Each triplet section depicts the data after normalization (a-d), the wavelet spectra (e-h) and the global wavelet spectra (blue) compared against a background red noise estimate (dashed red, i-l) Vertical dashed lines depict clusters identified as episodes of increased flood frequency.

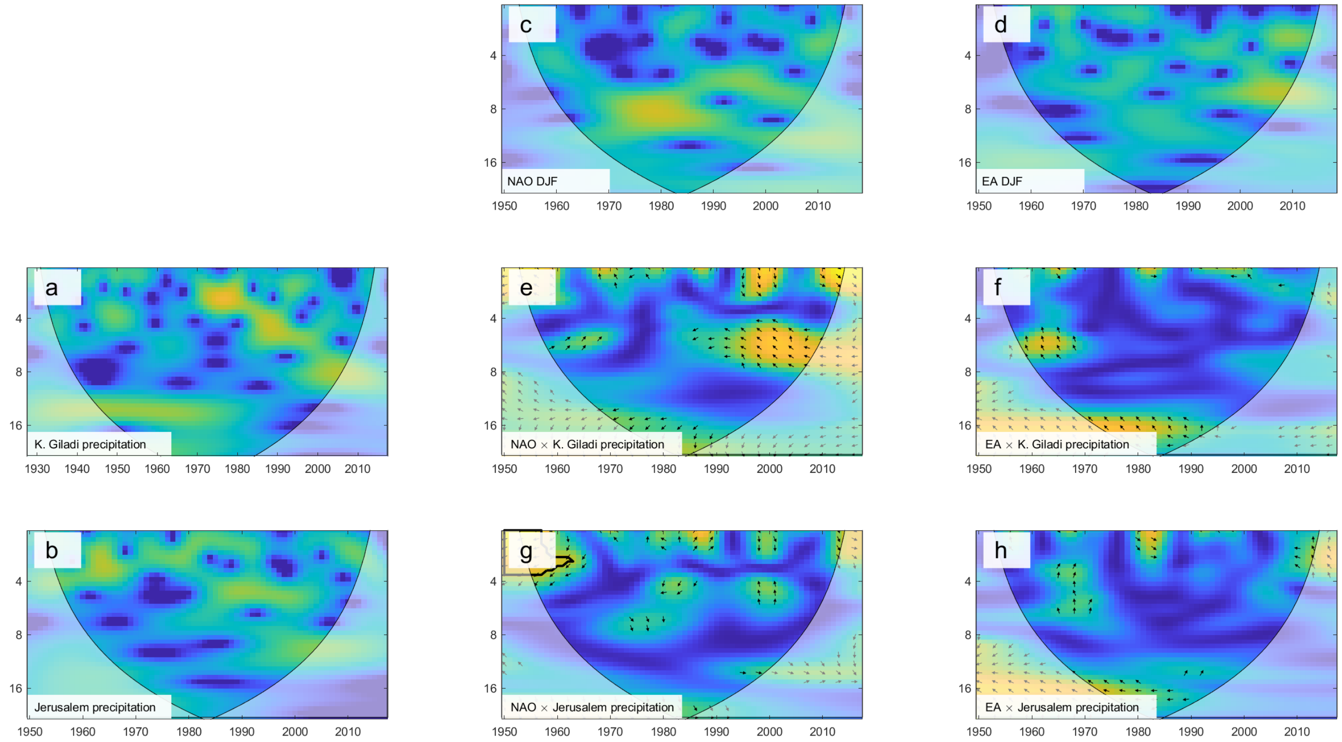

Figure S15 – wavelet (a-d) and wavelet coherence (e-h) analyses of modern annual precipitation in Kfar Giladi (a) and Jerusalem (b), and the North Atlantic Oscillation (c) (NOAA, 2020) and Eastern Atlantic (d) indices. The analyses are presented only for the times span when all data is available (1950-2018). Areas with significance level above 0.95 (α=0.05) are depicted by a black line. Arrows direction indicate the series interaction, with in-phase pointing right, anti-phase pointing left, and 90^{O} phase difference by vertical directions.

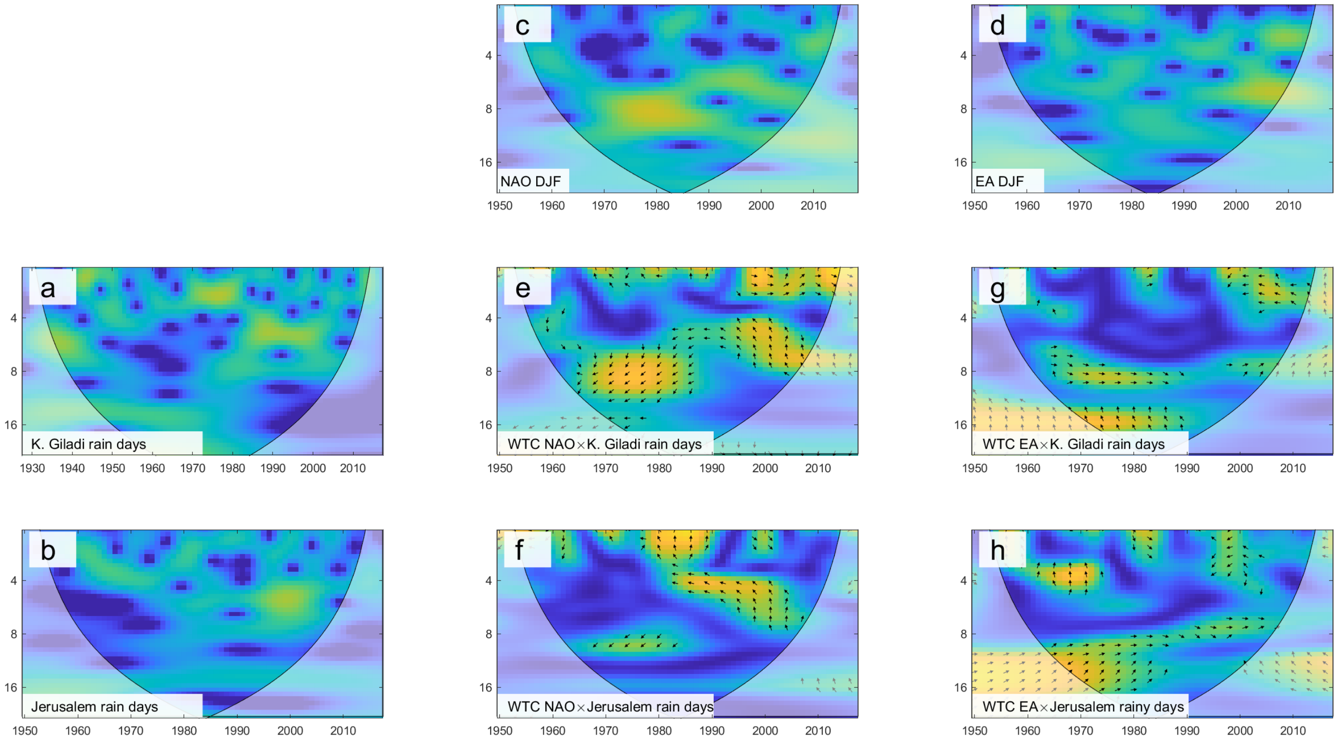

Figure S16 – wavelet (a-d) and wavelet coherence (e-h) the number of rainy days and winter (DJF) NAO and EA measured at Kfar Giladi station, and winter (DJF) NAO (c) and winter (DJF) EA indices (d; NOAA, 2020). Arrows indicate significance above 0.5, and areas with significance level above 0.95 (α=0.05) are depicted by a black line. Arrows direction indicate the series interaction, with in-phase pointing right, anti-phase pointing left, and 90^{O} phase difference by vertical directions.

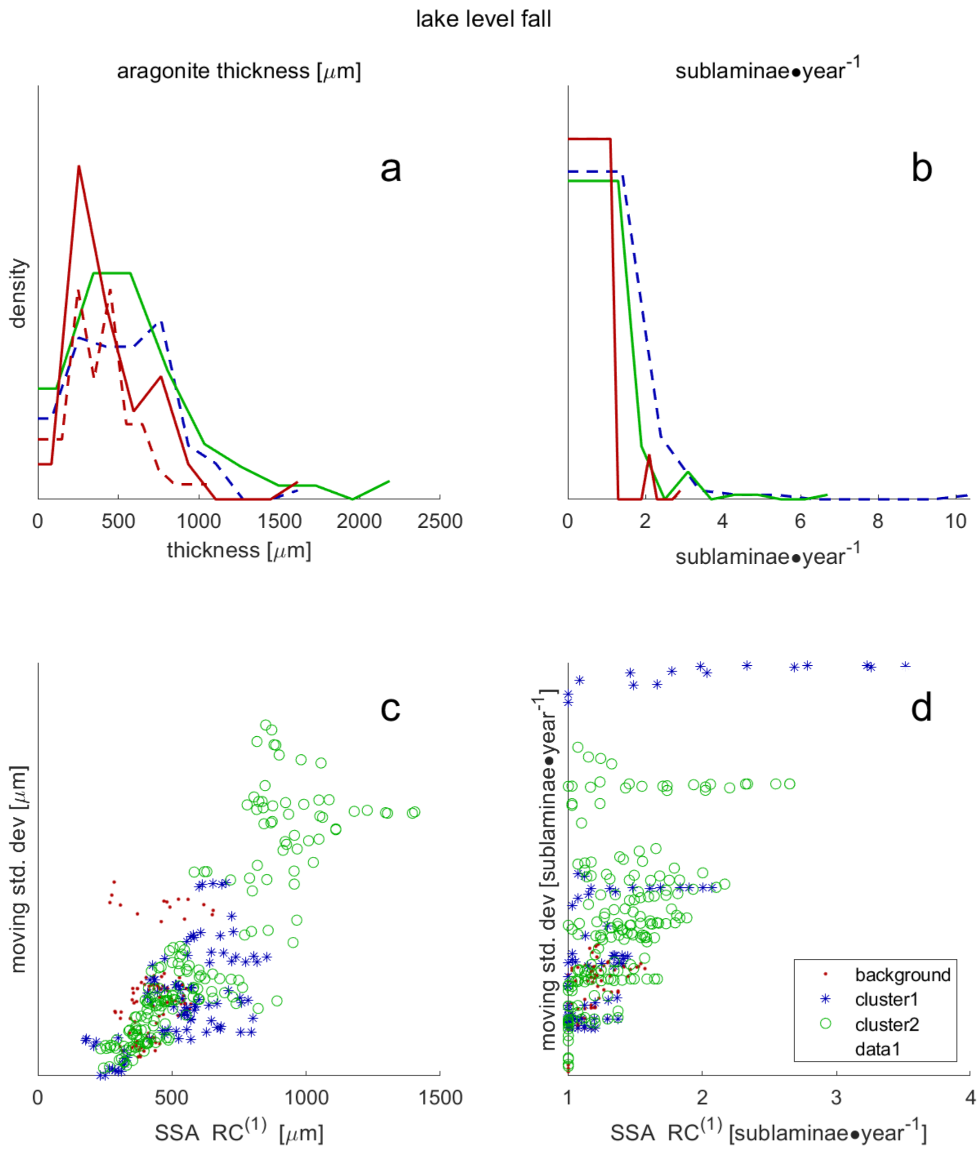

Figure S17 – distributions (a, b) and scatter (c, d) of statistical properties during studied falling lake level. Note the similarity between the first cluster and background intervals.

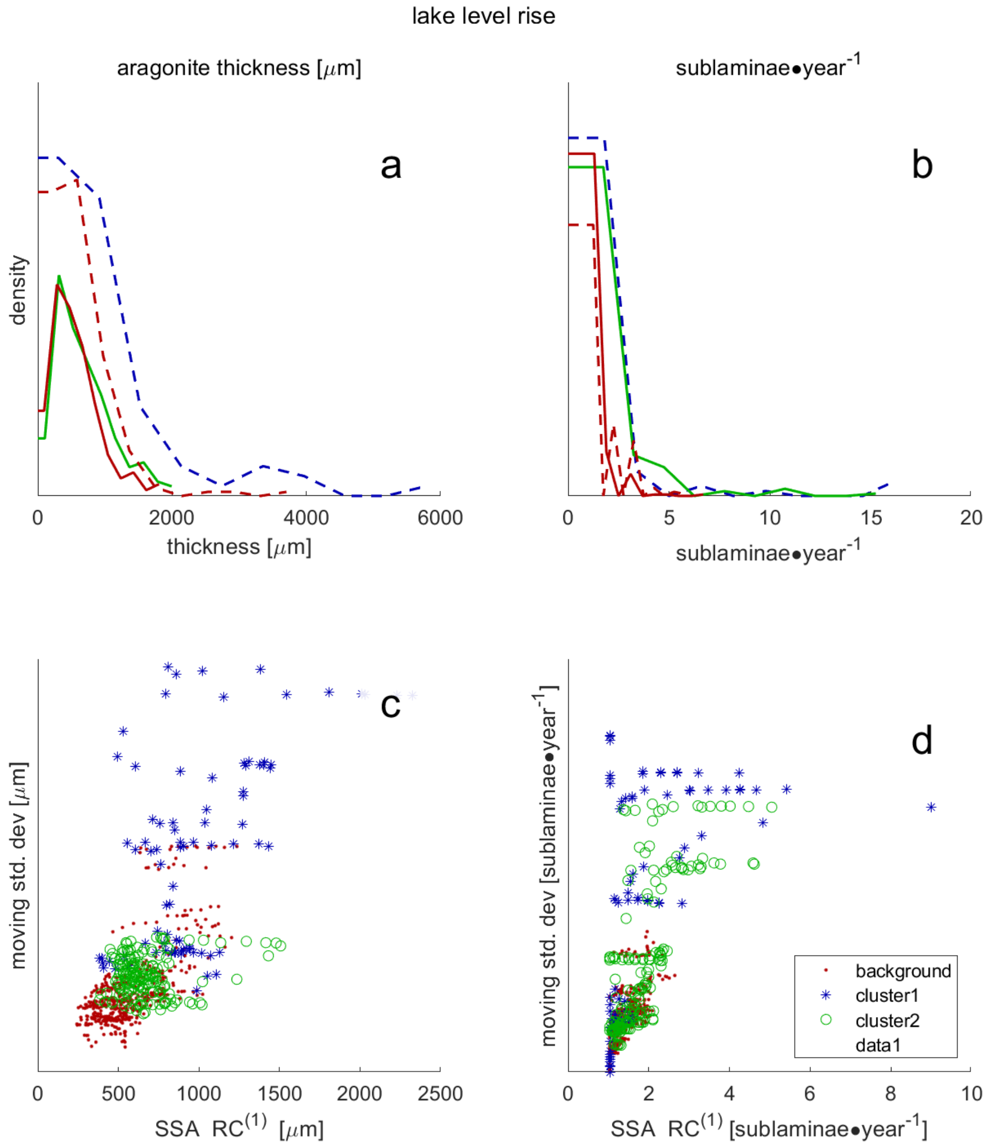

Figure S18 – distributions (a, b) and scatter (c, d) of statistical properties during studied falling lake level. Note the dissimilarity between the first cluster and the background intervals, and the similarity between the second cluster and the background intervals.